SRS-Induced Spatial-Spectral Distortion and Its Mitigation Strategy in High-Power Fiber Amplifiers

Chun Zhang, Lianghua Xie, Haokun Li, Benjian Shen, Xi Feng, Min Li, Rumao Tao, and Jianjun Wang

***Abstract*—The spatial-spectral evolution properties of laser beam in the presence of stimulated Raman scattering (SRS) effect have been studied in large mode area (LMA) fiber. With the employment of long/short pass filters, spatial evolution of the signal and Raman light has been studied individually. After the onset of SRS, the simultaneous optimizing of signal light and degrading of Raman light was observed, which has been attributed to the SRS effect of multimode laser beams in LMA fiber. The spectral evolution characteristics indicated that the SRS effect in LMA fiber will trigger other nonlinear effects, mainly inter-modal four-wave-mixing effect and cross-phase-modulation induced modulation instability. Furthermore, the impacts of bending strategy and multimode LMA fiber on SRS-induced spatial-spectral distortion have also been studied, which shows that the SRS-induced mode distortion can be suppressed by increasing the fiber size while the bending strategy plays a limited role.**

***Index Terms*—Fiber lasers, nonlinear optics, Raman scattering, four-wave mixing, brightness.**

I. Introduction

FOR continuous wave fiber laser systems, the stimulated Raman scattering (SRS) effect is one of the dominant nonlinear effects [1]. It is well known that the SRS effect results in the transfer of the signal power to Stokes light and the broadening of the linewidth asymmetrically [2]. Recently, a new phenomenon, named SRS-induced mode distortion, has also been observed in high power fiber lasers [3]–[5], which renders the single mode beam into a multi-mode operation and deteriorates the spatial brightness severely. The phenomenon was first observed by Hejaz *et al.* [3], and Chu *et al.* [4] studied the corresponding temporal-frequency characteristics, which revealed that SRS-induced mode distortion fluctuates on a time scale of seconds. SRS-induced mode distortion has become another major limitation for further power scaling of fiber lasers with near diffraction limited beam quality. However, the underlying physical mechanism is still under debate. Although the spatial as well as the temporal-frequency characteristics have been studied, the signal and Raman light has not been investigated individually, which may cause confusion in understanding the physical nature. Besides, with the presence of SRS-induced mode distortion, various mode-related nonlinear effects occur synchronously, which also result in the deterioration of the spectrum and cause the energy dispersion of the output laser. The SRS-induced spectral distortion further limits the laser applications, especially in the field of spectral beam combination [6]. However, the existing researches mainly focus on the SRS-induced mode distortion while there are few studies about spectral evolution. Thus, it is necessary to study and suppress SRS-induced spatial-spectral distortion.

In this work, the spatial-spectral evolution properties of laser beam in the presence of SRS effect have been experimentally studied separately for the first time, which revealed that SRS effect can induce abundant spatial-spectral behaviors in few-mode large mode area (LMA) fibers. Based on the physical mechanism, bending strategy and multimode LMA fiber have been employed to suppress SRS-induced spatial-spectral distortion. However, bending strategy can only suppress SRS-induced spectral distortion and result in obvious power reduction. The multimode LMA fiber can effectively suppress SRS-induced spatial-spectral distortion without any drawback.

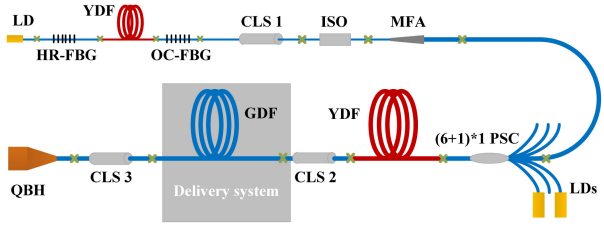

Fig. 1. Experimental setup of the laser system.

II. Experimental Setup

The architecture of the experimental setup is shown in Fig. 1, which consisted of a master oscillator power amplifier (MOPA) and a fiber-optic delivery system. A linear-cavity oscillator acted as the seed, which consisted of a piece of 4 m 10/130 double-clad Yb-doped fiber (YDF), a pair of high reflector (HR) and output coupler (OC) fiber Bragg grating (FBG), centered

Manuscript received December 12, 2021; revised January 24, 2022; accepted February 3, 2022. Date of publication February 8, 2022; date of current version March 2, 2022. This work was supported by the National Natural Science Foundation of China under Grant 61905226. *(Chun Zhang, Lianghua Xie, and Rumao Tao contributed equally to this work.) (Corresponding author: Rumao Tao.)*

Chun Zhang is with the Department of Optics and Optical Engineering, University of Science and Technology of China, Hefei 230026, China, and also with the Laser Fusion Research Center, China Academy of Engineering Physics, Mianyang 610200, China (e-mail: wsrf@mail.ustc.edu.cn).

Lianghua Xie, Haokun Li, Benjian Shen, Xi Feng, Min Li, Rumao Tao, and Jianjun Wang are with the Laser Fusion Research Center, China Academy of Engineering Physics, Mianyang 610200, China (e-mail: xielhthu@163.com; lihaokun182@163.com; shenbj@163.com; xifengsdu@126.com; limincaep@163.com; taorumao@sohu.com; wjjcaep@126.com).

This article has supplementary downloadable material available at https://doi.org/10.1109/JPHOT.2022.3149348, provided by the authors.

Digital Object Identifier 10.1109/JPHOT.2022.3149348

at 1075 nm. To stimulate the SRS effect intentionally, narrow linewidth FBG was employed [7], and the 3 dB linewidth of HR-FBG and OC-FBG were 0.3 nm and 0.07 nm, respectively. A 50 W fiber-pigtailed 976 nm laser diode (LD) was used to pump the oscillator. A homemade cladding light stripper (CLS) was used to strip the residual pump light and cladding signal light [8]. An isolator (ISO) was used to block off the backward light from the main amplifier and protect the oscillator. Then, a mode field adapter (MFA) was used to excite the fundamental mode and maintain nearly diffraction-limited beam quality in the main amplifier. The main amplifier consisted of a double-clad LMA YDF with a core/clad diameter of 20 um/400 um, and the core numerical aperture (NA) was about 0.06, which was coiled tightly in spiral configuration with the minimum and maximum bend diameters being 0.08 m and 0.17 m to suppress TMI (transverse mode instability) effectively [9]. The cladding absorption coefficient of the YDF is about 0.45 dB/m at 915 nm while the length is 12 m to ensure the total absorption coefficient of more than 16 dB. Co-pumping scheme has been employed in main amplifier due to lower SRS threshold [10]. Thirteen fiber-pigtailed non-wavelength-stabilized 976 nm laser diodes have been combined by 7 $\times$ 1 pump combiner into two groups, which were used to pump the YDF through a forward (6+1) $\times$1 pump/signal combiner (PSC). The maximum pump power was about 1.27 kW. Another two homemade CLSs were employed to strip the residual pump laser and cladding mode signal laser. It should be mentioned that, after the CLS 2, the amplified fiber laser has passed through an extra monolithic fiber-optic delivery system for the purpose of power delivering as well as triggering the SRS effect, which was terminated with a home-made anti-reflection coated collimated quartz block head (QBH) for suppressing the deleterious backward reflection [11].

To investigate the laser performance, the output power, optical spectrum, temporal characteristics and beam quality have been recorded. The output power is measured by a water-cooled power meter, the calibration error of which is less than $\pm$2%. The spectrum of output laser is measured by an optical spectrum analyzer with the resolution of 0.1 nm. The temporal characteristics have been studied by using a photodiode (PD) with a hole of 1.0 mm diameter and bandwidth of 14 MHz, and a charge-coupled device (CCD) with 20 Hz sampling rate has also been employed to study the temporal characteristics of the beam profiles. The PD-measured time traces have been recorded by detecting the scattering light from the power meter, which agree well with those sampled the small spatial portion of low-power beam profile directly [12], and has been employed in Ref. [13] and [14]. Beam quality (M^2) was measured by a M^2 meter with the D4σ definition [15], and the typical accuracy of M^2 meter is less than $\pm$5%. It should be mentioned that a pair of short pass and long pass filters have also been employed to separate the Raman light and the signal light, both of which have the cut-off wavelength around 1100 nm.

III. Experimental Results

The output performances of MOPA without extra delivery system have been studied at first. The output power reached 917 W when the injected pump power raised to 1271 W. Measured

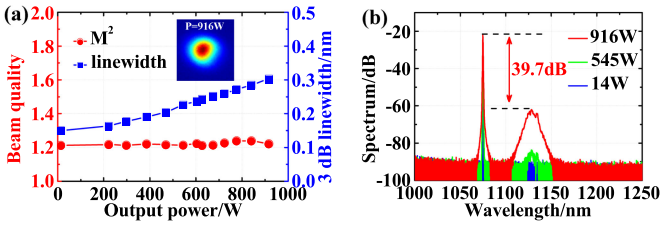

Fig. 2. (a) The beam quality and 3 dB linewidth evolution; (b) the spectral evolution of MOPA without delivery system.

spatial-spectral evolutions are shown in Fig. 2. One can see that the M^2 was nearly constant, which was slightly larger than 1.2. The stability of laser beam has been studied by PD at first, and none TMI has been observed [16]. Furthermore, the far-field and near-field beam profile (Visualization 1) was measured by a low-speed charge-coupled device (CCD) with 20 Hz sampling rate, which also remained stable. It should be mentioned that the movement of far-field beam profile mainly attributed to the perturbation of the environment noise, such as the turbulence, mechanical vibration, ect. [4]. The spectral evolution is plotted in Fig. 2(b). Once the output power reached 545 W, the characteristic peaks of 1st Raman effect appeared, which exhibit the typical shape of Raman gain spectrum [2]. At the maximal output power, the signal to Raman noise ratio (RSNR) was 39.7 dB. One can also see from Fig. 2(b) that the broadening of signal peak is nearly symmetric, which means that the broadening wasn't induced by the SRS effect [2]. The 3 dB linewidth as a function of operation power is also shown in Fig. 2(a), which increased linearly as the operation power increased due to the influence of self-phase modulation (SPM) [17], [18]. Thus, one can conclude that the impacts of SRS effect on spatial-spectral characteristics is negligible at this moment.

To stimulate the SRS-induced mode distortion, an extra 15 m 20/400 LMA Ge-doped fiber (GDF) with 0.4 m bending diameter was spliced between MOPA and CLS 3 to enhance the nonlinear effects. With the increase of interplay distance, SRS effect enhanced significantly, and other nonlinear effects occurred, mainly SRS-induced cross-phase-modulation induced modulation instability (XPM-MI), and IM-FWM effect, as shown in Fig. 3(a). Firstly, the characteristic peaks of 1st Raman effect have been observed when the output power reached 283 W. Then, two sidelobes around the signal wavelength appeared at 1067.9 nm and 1081.4 nm as the power scaled to 366 W, which manifested the appearance of SRS-induced XPM-MI [2]. The calculated gain spectra [2], [19] of SRS-induced XPM-MI effect is plotted in Fig. 3(b). One can see that the gain peak is located near 1.53 THz, and the corresponding stokes and anti-stokes light is around 1080.7 nm and 1068.9 nm, respectively, which agrees well with the experimental results. Meanwhile, the Stokes line at the wavelength of 1096.6 nm and the anti-Stokes line at 1053.2 nm have also been observed, which indicated the presence of IM-FWM effect. The phase-matching condition [20] was calculated and plotted in Fig. 3(c), which indicated that the frequency shift of IM-FWM is 5.4 THz, and the involved modes was 1074.8 nm (LP_{01},LP_{11}) $\rightarrow$ 1054.4 nm (LP_{01}) + 1096.0 nm (LP_{11}). With the power further increased to 593 W, 2nd SRS

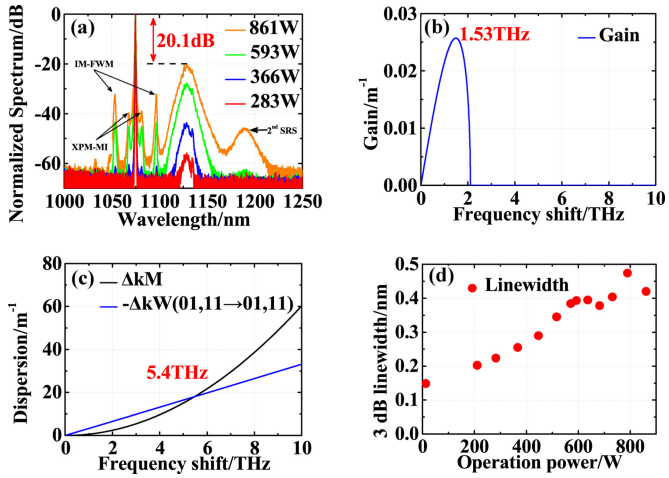

Fig. 3. (a) The normalized spectral evolution; (b) gain spectra of SRS-induced XPM-MI; (c) phase-match diagrams of IM-FWM; (d) 3 dB linewidth -evolution of MOPA with extra 15 m 20/400 delivery GDF under 0.4 m bending diameter.

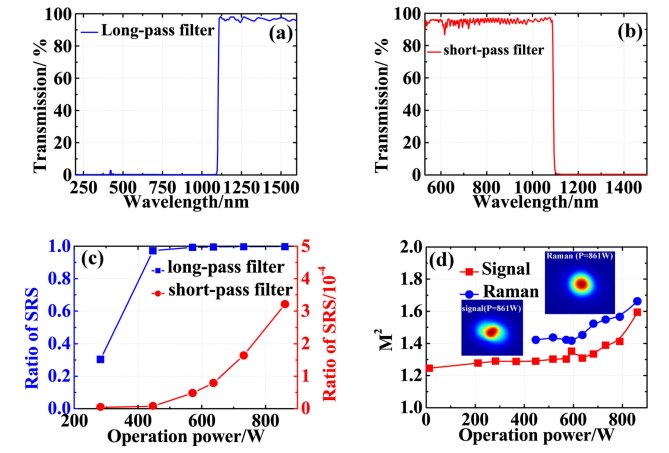

Fig. 4. (a) The transmission profile of long pass filters; (b) the transmission profile of short pass filters; (c) the power fraction evolutions of Raman stokes light with the employment of filters; (d) the beam quality (M2) evolution of MOPA with extra 15 m 20/400 delivery GDF under 0.4 m bending diameter.

has been observed. At maximal operation power, the RSNR was reduced to 20.1 dB. Meanwhile, the SNR of signal light to both the XPM-MI and IM-FWM effects' are higher than 30 dB at the maximal operation power, the strength of which are much weaker than SRS effect. Thus, the impacts of XPM-MI and IM-FWM effect on spatial measurements are negligible.

Also, the 3 dB linewidth as a function of operation power is shown in Fig. 3(d). After splicing 15 m GDF, the linearly broadening of the linewidth at low operation power was also induced by SPM. As the power scaled beyond 366 W, the impacts of SRS effect became visible, which led to the nonlinearly linewidth broadening [2]. Then, with the SRS-induced mode distortion, the beam profile no longer kept Gaussian shape but fluctuated at the second-level [4], which will be discussed in the next part. Due to the impacts of beam distortion and fluctuation, the evolution of spectrum broadening into chaos [18].

To study the spatial evolution properties of signal and Raman light individually, a pair of short/long pass filters have been used to separate the signal and Raman light. Fig. 4(a) and (b) show the transmission profile of filters, which reveals that the cut-off wavelength of both filters are around 1100 nm. Fig. 4(c) illustrates the power fraction evolutions of Raman stokes light under the employment of filters, which was calculated by the spectral integration from 1100 nm to 1170 nm. Combined the results in Fig. 3(a) with Fig. 4(c), one can see that, with the help of long-pass filter, the Raman light can be separated effectively even with 35.9 dB RSNR, and the short-pass filter can filter Raman light effectively. Fig. 4(d) shows the spatial evolution properties. The signal beam distortion became obvious with power scaling beyond 571 W. At the maximal operation power, signal light M^2 degraded gradually to 1.6, and the beam profile no longer kept Gauss shape, as the insert fig in Fig. 4(d) shows. The Raman light beam quality evolution and beam profile at the maximal output power have also been plotted in Fig. 4(d). One can note that the signal beam quality evolution around the 593 W output power seems abnormally: the beam quality distorted obviously at 593 W while improved at 637 W. To avoid the influence of measurement error, the beam quality data has been measured repeatedly, and the abnormal behavior remains. One can also see that the Raman light beam quality also degraded once the operation power below 593 W. One possible explanation for this behavior is the SRS effect of multimode laser beams. In Ref. [4], the SRS-induced mode distortion was attributed to the core-pumped Raman effect. With a larger effective mode area, the Raman threshold of HOMs is higher than FM. Before the output power reached 593 W, only the FM signal light reached Raman threshold, with the presence of core-pumped Raman effect, the FM signal light distorted to HOMs while the stimulated Raman light was in FM content [4]. As the power scaling, HOMs also reached Raman threshold, which consumed the signal HOMs and weakened the SRS-induced mode distortion. This results in that the M^2 of signal light reduced when the operation power scaled above 593 W. Meanwhile, HOMs signal light generated the HOMs Raman light and distorted Raman beam quality, which results in the increase of M^2 for Raman light. As the operation power increased above 637 W, the consuming of HOMs has been outweighed by the generating of HOMs, which leads to that the M^2 of signal light and Raman light degraded continuously. It should be mentioned that, due to the beam cleanup effect induced by core-pumped Raman effect, the Raman light beam profile mainly existed in the FM distribution [4], [21]. However, the Raman light has a higher M^2 value than the signal light. This is due to that the wavelength range of anti-reflection coated collimated QBH has not cover the Raman light, which results to that part of the Raman light reflected by the output interface of the QBH and became random stray light. Some of the random stray light finally reached the CCD, and formed a background around the main beam spot. Due to the M^2 was measured with the D4σ definition, the presence of background light results to that the measured beam size is larger than the real size of Raman light, which results in that the base of Raman light beam quality was around 1.4 and larger than that of the signal laser.

The stability of laser beam has also been studied by PD at first. The Fourier analysis has been applied on the time traces to calculate the corresponding Fourier spectra (FS) [12]. Fig. 5(a) shows the FS results at different operation power. Similar to Ref. [4], no

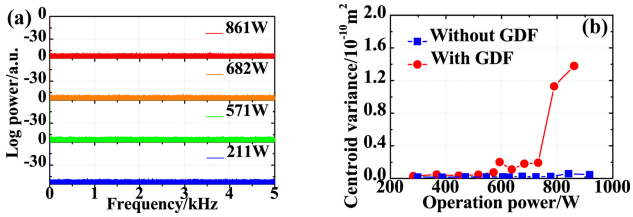

Fig. 5. (a) The Fourier spectrum of time traces; and (b) the variance of signal's centroid at different operation power of MOPA with extra 15 m 20/400 delivery GDF under 0.4 m bending diameter.

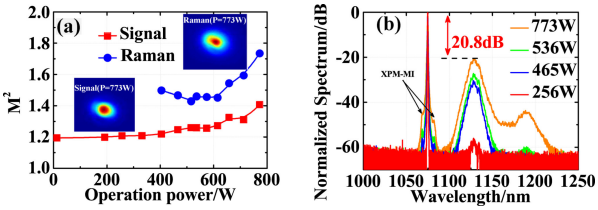

Fig. 6. The spatial-spectral evolution properties: (a) beam quality (M2); (b) normalized spectrum of MOPA with 15 m 20/400 delivery GDF under 0.12 m bending diameter.

characteristic TMI frequency component has shown up, which means that the laser system is free of Raman-induced TMI and the beam profile evolution can be recorded by a low-speed CCD accurately. Both the far-field and near-field signal beam profile (Visualization 2) fluctuated at the second-level time scale, and the fluctuation at near-field was more visible. To quantitatively study the SRS-induced mode distortion, the variances of signal light's centroid at near-field have been calculated and plotted in Fig. 5(b). Besides, the results of MOPA without extra GDF have also been plotted for comparison. One can see that the variances increase after the output power beyond 593 W, and the increase became significantly once the operation power reached 731 W. Besides, the Raman light beam profile has also been measured at far-field (Visualization 3), which mainly existed in FM distribution, and none obvious fluctuation.

To suppress SRS-induced spatial-spectral distortion, bending strategy has been employed at first, and the results are plotted in Fig. 6. With the bending diameter of extra GDF reduced from 40 cm to 12 cm, part of HOMs leaked to the cladding and stripped by CLS 3, which results in the output power decreased by 10%. In theory, with the stripping of HOMs, beam quality can be improved and the IM-FWM effect can be suppressed [20], which means that SRS-induced spatial-spectral distortion can be mitigated. Before decreasing the bending diameter of extra GDF, signal light M^2 was 1.41 at 781 W output, as Fig. 4(b) shows. However, with the employment of bending strategy, signal light M^2 also reached 1.41 at 773 W maximal output though part of HOMs was stripped. Besides, the measured signal beam profile evolution results (Visualization 4) show that the beam fluctuation didn't be suppressed. Even worse, the Raman light demonstrated a more severe beam degradation and fluctuation (Visualization 5). Thus, one can conclude that bending strategy has limited impacts on SRS-induced spatial distortion. The impacts of bending strategy on SRS-induced spectral distortion has also been studied. With the strip of HOMs, IM-FWM effect and XPM-MI effect were suppressed effectively while the RSNR only decreased by 0.7 dB.

After reconsidering the physical mechanism of SRS-induced spatial-spectral distortion, the invalidation of bending strategy can be explained by the core-pumped Raman effect and bending-induced mode shrinking [22]. Besides increasing the leaking loss of HOMs, bending strategy can also induce mode shrinking and decrease the effective mode area. As an intensity-dependent nonlinear effect, SRS effect gets strengthened with the decrease of mode area. Thus, the SRS effect in the fiber core center can be enhanced with the decrease of bending diameter, which leads to a stronger mode distortion [4]. Meanwhile, with the decrease of effective mode area, the inter-mode wave-mixing (IM-WM) effect among the signal FM and Raman HOMs would also be enhanced [23]. It is worth noting that the IM-WM effect described in Ref. [23] represents the power transform from the signal FM to the Raman HOMs. As a result, with the decrease of bending diameter, RSNR only decreased by 0.7 dB though the output power dropped by 10%, and signal light beam quality has not been improved while Raman light shows a more severe beam degradation.

Due to the bending strategy plays a limited role in suppressing SRS-induced spatial-spectral distortion, and all of the relevant nonlinear effects depend on the power intensity [2]. As a common suppression strategy, highly multimode fiber can expand the effective mode area and mitigate intensity-depended nonlinear effects effectively [24]–[28]. Thus, the 20/400 LMA GDF was replaced with an equal length 50/400 multimode LMA GDF [29], which had the core NA of 0.11 and was coiled tightly in spiral configuration to avoid the HOMs excited by the scattering from the bent fiber [30], [31]. The bending diameter of 50/400 multimode LMA GDF was 0.2 m, which has limited impacts on the output performances and would be explained by the stronger HOMs constraint capacity of 50/400 highly multimode GDF [29], [32]. Considering that the normalized frequency V is 3.8 for 20/400 GDF while equal to 17.07 for 50/400 GDF, there are only LP_{01} and LP_{11} modes be supported in the 20/400 GDF while there are 18 modes be supported in 50/400 GDF. To avoid HOMs excitation at the fusion splice, a home-made 20/400-to-50/400 MFA has been employed [32]. As the core size increases, the taper length of the multimode LMA fiber in the MFA should be increased, which increases the complexity and cost of the MFA fabrication. On the other hand, as the core diameter increases, the length maintaining beam quality reduces as shown in Ref. [29]. The ultimate limitation is the conjunction of mode field adapting technology and the required length to maintain the beam quality.

The spatial-spectral evolution properties are plotted in Fig. 7. From Fig. 7(a), one can see that the beam quality remained stable until the operation power beyond 760 W and reached 1.5 at maximal output power. Besides, beam profile evolution of signal light (Visualization 6) and Raman light (Visualization 7) have also been measured, both of which were nearly stable and further proved that the SRS-induced spatial distortion has been suppressed effectively. Meanwhile, with the expansion of effective mode area, all of the nonlinear effects have been suppressed effectively, none of the XPM-MI and IM-FWM effect have been observed while the RSNR decreased to 27.4 dB at

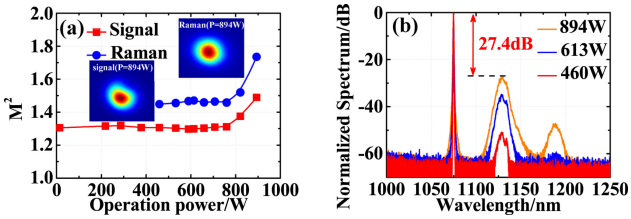

Fig. 7. The spatial-spectral evolution properties: (a) normalized spectra; (b) beam quality (M^2) of MOPA with 15 m 50/400 multimode delivery GDF.

maximal operation power. In addition, the mitigation of SRS-induced XPM-MI has also been attributed to the suppression of SRS effect while the inhibition of IM-FWM is also attributed to the improvement of beam quality.

IV. Conclusion

In conclusion, SRS-induced spatial-spectral distortion has been studied and mitigated in LMA fiber amplifiers. The experimental results indicated that the SRS effect in LMA fiber not only induces signal light and Raman light degradation and fluctuation, but also triggers other nonlinear effects, mainly IM-FWM and SRS-induced XPM-MI. Besides, the spatial evolution results also show that the SRS effect of multimode laser beams can result in the mode coupling between the signal light and Raman light in few-mode LMA fibers. To suppress SRS-induced spatial-spectral distortion, bending strategy and multimode LMA fiber have been employed. However, the bending strategy has a limited impact on suppressing SRS-induced spatial distortion and results in obvious power reduction, which can be explained by the bending-induced mode shrinking. With the expansion of effective mode area, the SRS effect and SRS-induced spatial-spectral distortion got suppressed.

Acknowledgment

The authors acknowledge Yu Liu, Shan Huang, Wenjie Wu, and Huaqing Song for manufacturing of fiber components, and the authors also want to acknowledge Qiuhui Chu for helpful discussions on fiber amplifier construction.

References

[1] M. N. Zervas and C. A. Codemard, "High power fiber lasers: A review," *IEEE J. Sel. Top. Quantum Electron.*, vol. 20, no. 5, Sep./Oct. 2014, Art. no. 0904123.

[2] G. Agrawal, *Nonlinear Fiber Optics*, 4th ed. San Diego, CA, USA: Academic Press, 2006, pp. 274–328.

[3] K. Hejaz *et al.*, "Modal instability induced by stimulated Raman scattering in high-power Yb-doped fiber amplifiers," *Opt. Lett.*, vol. 42, no. 24, pp. 5274–5277, Dec. 2017.

[4] Q. H. Chu *et al.*, "Experimental study of mode distortion induced by stimulated Raman scattering in high-power fiber amplifiers," *Photon. Res.*, vol. 8, no. 4, pp. 595–600, Apr. 2020.

[5] W. Gao *et al.*, "Effective suppression of mode distortion induced by stimulated Raman scattering in high-power fiber amplifiers," *High Power Laser Sci. Eng.*, vol. 9, May 2021, Art. no. e20.

[6] M. Jiang, P. F. Ma, P. Zhou, and X. L. Wang, "Beam quality in spectral beam combination based on multi-layer dielectric grating," *Acta Physica Sinica*, vol. 65, no. 10, May 2016, Art. no. 104203.

[7] W. Liu, P. Ma, H. Lv, J. Xu, P. Zhou, and Z. Jiang, "General analysis of SRS-limited high-power fiber lasers and design strategy," *Opt. Exp.*, vol. 24, no. 23, pp. 26715–26721, Nov. 2016.

[8] Y. Liu *et al.*, "2 kW high stability robust fiber cladding mode stripper with moderate package temperature rising," *IEEE Photon. Technol. Lett.*, vol. 32, no. 18, pp. 1151–1154, Sep. 2020.

[9] R. Tao, R. Su, P. Ma, X. Wang, and P. Zhou, "Suppressing mode instabilities by optimizing the fiber coiling methods," *Laser Phys. Lett.*, vol. 14, no. 2, Feb. 2017, Art. no. 025101.

[10] C. Shi *et al.*, "Experimental study of output characteristics of bi-directional pumping high power fiber amplifier in different pumping schemes," *IEEE Photon. J.*, vol. 9, no. 3, Jun. 2017, Art. no. 1502910.

[11] Y. Ye *et al.*, "Experimental study of 5-kW high-stability monolithic fiber laser oscillator with or without external feedback," *IEEE Photon. J.*, vol. 11, no. 4, Aug. 2019, Art. no. 1503508.

[12] R. Tao, P. Ma, X. Wang, P. Zhou, and Z. Liu, "Study of mode instabilities in high power fiber amplifiers by detecting scattering light," in *Proc. Int. Photon. Optoelectron. Meetings*, Wuhan, China, 2014, Paper FTh2F.2.

[13] R. Tao, P. Ma, X. Wang, P. Zhou, and Z. Liu, "Comparison of the threshold of thermal-induced mode instabilities in polarization-maintaining and non-polarization-maintaining active fibers," *J. Opt.*, vol. 18, no. 6, 2016, Art. no. 065501.

[14] R. Tao, P. Ma, X. Wang, P. Zhou, and Z. Liu, "Study of dopant concentrations on thermally induced mode instability in high-power fiber amplifiers," *Laser Phys.*, vol. 26, no. 6, Jun. 2016, Art. no. 065103.

[15] A. E. Siegman, "How to (Maybe) measure laser beam quality," in *Proc. Diode Pumped Solid State Lasers: Appl. Issues*, WA, DC, USA, vol. 17, 1998, Paper MQ1.

[16] H.-J. Otto *et al.*, "Temporal dynamics of mode instabilities in high-power fiber lasers and amplifiers," *Opt. Exp.*, vol. 20, no. 14, pp. 15710–15722, Jul. 2012.

[17] W. Liu, W. Kuang, M. Jiang, J. Xu, P. Zhou, and Z. Liu, "Modeling of the spectral evolution in a narrow-linewidth fiber amplifier," *Laser Phys. Lett.*, vol. 13, no. 3, Mar. 2016, Art. no. 035105.

[18] R. Tao *et al.*, "Dynamic characteristics of stimulated raman scattering in high power fiber amplifiers in the presence of mode instabilities," *Opt. Exp.*, vol. 26, no. 19, pp. 25098–25110, Sep. 2018.

[19] M. Yan, Y. Zheng, H. Liang, F. Li, Z. Han, and R. Zhu, "Stokes light induced modulation instability in high power continuous wave fiber amplifiers," *Opt. Exp.*, vol. 29, no. 6, pp. 8407–8416, Mar. 2021.

[20] L. Yin, Z. Han, H. Shen, and R. Zhu, "Suppression of inter-modal four-wave mixing in high-power fiber lasers," *Opt. Exp.*, vol. 26, no. 12, pp. 15804–15818, Jun. 2018.

[21] H. Zhang, H. Xiao, X. Wang, P. Zhou, and X. Xu, "Mode dynamics in high-power yb-Raman fiber amplifier," *Opt. Lett.*, vol. 45, no. 13, pp. 3394–3397, Jul. 2020.

[22] R. T. Schermer, "Mode scalability in bent optical fibers," *Opt. Exp.*, vol. 15, no. 24, pp. 15674–15701, Nov. 2007.

[23] W. Liu, P. Ma, C. Shi, P. Zhou, and Z. Jiang, "Theoretical analysis of the SRS-induced mode distortion in large-mode area fiber amplifiers," *Opt. Exp.*, vol. 26, no. 12, pp. 15793–15803, Jun. 2018.

[24] S. Shaklan, "Selective mode injection and observation for few-mode fiber optics," *Appl. Opt.*, vol. 30, no. 30, pp. 4379–4383, Oct. 1991.

[25] C. D. Stacey, R. M. Jenkins, J. Banerji, and A. R. Davies, "Demonstration of fundamental mode only propagation in highly multimode fibre for high power EDFAs," *Opt. Commun.*, vol. 269, no. 2, pp. 310–314, Jan. 2007.

[26] S. Hurand, L.-A. Chauny, H. El-Rabii, S. Joshi, and A. P. Yalin, "Mode coupling and output beam quality of 100-400 mu core silica fibers," *Appl. Opt.*, vol. 50, no. 4, pp. 492–499, Feb. 2011.

[27] J.-P. Negel *et al.*, "Delivery of 800 w of nearly diffraction-limited laser power through a 100 m long multi-mode fiber," *Laser Phys. Lett.*, vol. 11, no. 5, May 2014, Art. no. 055104.

[28] C. Roehrer, G. Kleem, M. A. Ahmed, and T. Graf, "Analysis of fundamental-mode beam transport in highly multimode fibers," *J. Lightw. Technol.*, vol. 35, no. 17, pp. 3637–3642, Sep. 2017.

[29] C. Rohrer, C. A. Codernard, G. Kleem, T. Graf, and M. A. Ahmed, "Preserving nearly diffraction-limited beam quality over several hundred meters of transmission through highly multimode fibers," *J. Lightw. Technol.*, vol. 37, no. 17, pp. 4260–4267, Sep. 2019.

[30] A. W. Snyder and J. D. Love, *Optical Waveguide Theory*. Boston, MA USA: Springer, 1983, pp. 542–566.

[31] W. Liu, J. Cao, and J. Chen, "Study on the adiabaticity criterion of the thermally-guided very-large-mode-area fiber," *Opt. Exp.*, vol. 26, no. 7, pp. 7852–7864, 2018.

[32] R. Tao *et al.*, "Simple one-step-tapering 20 μm-to-50 μm monolithic MFA for long-distance high-power laser transmission applications," in *Proc. Conf. Lasers Electro-Opt.*, San Jose, CA, USA, 2021, Paper AW4D.4.